molecules

MDPI

Article

New Non-Fullerene Acceptor with Extended Conjugation of Cyclopenta [2,1-b:3,4-b′] Dithiophene for Organic Solar Cells

Cheng Sun [1,†], Sanseong Lee [2,3,†], Changeun Choi [4], Soyeong Jeong [3], Juhui Oh [2,3], Ju-Hyeon Kim [2,3], Jaeyoung Kim [2,3], Ho Eon Baek [1], Hongkyu Kang [5], Soo-Young Jang [6,*], Hyun Ho Choi [4,*], Kwanghee Lee [2,3,*] and Yun-Hi Kim [1,*]

1 Department of Chemistry and RIGET, Gyeongsang National University, Jinju 52828, Korea
2 School of Materials Science and Engineering, Gwangju Institute of Science and Technology, Gwangju 61005, Korea
3 Heeger Center for Advanced Materials, Research Institute for Solar and Sustainable Energies, Gwangju Institute of Science and Technology, Gwangju 61005, Korea
4 Department of Materials Engineering and Convergence Technology and RIGET, Gyeongsang National University, Jinju 52828, Korea
5 Center for Research Innovation, Gwangju Institute of Science and Technology, Gwangju 61005, Korea
6 Research Institute for Solar and Sustainable Energies, Gwangju Institute of Science and Technology, Gwangju 61005, Korea
* Correspondence: syjang@gist.ac.kr (S.-Y.J.); hh.choi@gnu.ac.kr (H.H.C.); klee@gist.ac.kr (K.L.); ykim@gnu.ac.kr (Y.-H.K.)
† These authors contributed equally to this work.

Abstract: Herein, we design and characterize 9-heterocyclic ring non-fullerene acceptors (NFAs) with the extended backbone of indacenodithiophene by cyclopenta [2,1-b:3,4-b′] dithiophene (CPDT). The planar conjugated CPDT donor enhances absorption by reducing vibronic transition and charge transport. Developed NFAs with different end groups shows maximum absorption at approximately 790–850 nm in film. Because of the electronegative nature of the end-group, the corresponding acceptors showed deeper LUMO energy levels and red-shifted ultraviolet absorption. We investigate the crystallinity, film morphology, surface energy, and electronic as well as photovoltaic performance. The organic photovoltaic cells using novel NFAs with the halogen end groups fluorine or chlorine demonstrate better charge collection and faster exciton dissociation than photovoltaic cells using NFAs with methyl or lacking a substituent. Photovoltaic devices constructed from m-Me-ITIC with various end groups deliver power conversion efficiencies of 3.6–11.8%.

Keywords: non-fullerene acceptor; cyclopenta [2,1b:3,4b′] dithiophene; organic solar cell; surface energy; film morphology; ITIC

check for updates

Citation: Sun, C.; Lee, S.; Choi, C.; Jeong, S.; Oh, J.; Kim, J.-H.; Kim, J.; Baek, H.E.; Kang, H.; Jang, S.-Y.; et al. New Non-Fullerene Acceptor with Extended Conjugation of Cyclopenta [2,1-b:3,4-b′] Dithiophene for Organic Solar Cells. *Molecules* **2022**, *27*, 7615. https://doi.org/10.3390/molecules27217615

Academic Editor: Barbara Panunzi

Received: 26 October 2022
Accepted: 3 November 2022
Published: 6 November 2022
Corrected: 9 March 2026

Publisher's Note: MDPI stays neutral with regard to jurisdictional claims in published maps and institutional affiliations.

Copyright: © 2022 by the authors. Licensee MDPI, Basel, Switzerland. This article is an open access article distributed under the terms and conditions of the Creative Commons Attribution (CC BY) license (https://creativecommons.org/licenses/by/4.0/).

1. Introduction

Organic solar cells (OSCs) are regarded as next-generation photovoltaics because their advantages of lightweight, semi-transparent, tunable energy levels and absorption range, and potential application for flexible devices [1–8]. A typical bulk heterojunction (BHJ) organic solar cell is a combination of acceptor and donor materials. In the early stage of organic solar cells, fullerene derivatives were used as acceptors, owing to their excellent electron and affinity mobility and appropriate nanoscale morphology. [9–14] Benefits from the development of device optimization and donor materials [15–20], fullerene-based OSCs have exceeded 10% power conversion efficiencies (PCEs) [21,22]. However, limitations such as inferior near-infrared and narrow visible region absorption as well as low tunability of energy level have limited the further development of fullerene derivatives [23–25].

To overcome the limitations of fullerene derivatives, ITIC non-fullerene acceptors (NFAs) and their derivatives with acceptor-donor-acceptor (A-D-A) architecture have drawn particular interest owing to broad light absorption, regulable energy levels, stable

morphological, and low-cost synthesis potential [26–33]. This A-D-A backbone includes a fused and planar electron-donating unit capped with electron-withdraw end groups. Through manipulation of the backbone conjugated length [34–38], sidechain type and length [39–43], and end groups [44,45], the electronic and morphological properties can easily modify. With the boost of ITIC non-fullerene acceptor, the PCEs of organic solar cells have reached 13–15% [46–53].

In this paper, we utilize extended conjugation: the conjugation of indacenodithiophene is extended by substituting the outward thienothiophene moieties with cyclopenta [2,1-b:3,4-b′] dithiophene (CPDT), which enables construction 9-heterocyclic ring acceptor, meta-methyl-ITIC (m-Me-ITIC). The symmetric and planar conjugated CPDT electron rich moiety enhances absorption because of reduced vibronic transition and enhances the charge transport. Additionally, extended conjugate bridging units improved the absorption in the long-wavelength region. Meta-alkoxy phenyl side chains provide good solubility in common solvents, and different end groups lead to distinct LUMO energy levels with good morphology in the film state [28]. Blend with PBDB-T polymer donor, the m-Me-ITIC device delivers an open-circuit voltage (Voc) of 0.78 V, and short-circuit current density (Jsc) of 23.7 mA·cm^{-2}, fill factor (FF) of 64%, and PCE of 11.8%.

2. Experimental

2.1. Synthesis

2.1.1. Synthesis of Compound **2**

n-BuLi (5.4 mL, 13.5 mmol) was dropped into THF solution of 1-bromo-3-((2-ethylhexyl) oxy)benzene (6.0 g, 13.1 mmol) at −78 °C and string for 1.5 h. Compound **1** (2 g, 2.2 mmol) was added to the mixture, and after stirred at 25 °C overnight, the solvent was removed. The crude product was added to 100 mL THF with 10 g amberlyst® 15(H) and stirred for 1 h at 70 °C after cooling down to temperature and removing the solvent, crude purified with silica gel chromatography (hexane/dichloromethane 9:1) to give compound **2** (1.9 g, 65%).

^{1}H NMR (300 MHz, $CDCl_3$) δ 7.26 (s, 4H), 7.13 (t, *J* = 8.0 Hz, 4H), 7.00 (t, *J* = 2.0 Hz, 4H), 6.88 (d, *J* = 7.9 Hz, 4H), 6.83 (d, *J* = 4.6 Hz, 2H), 6.77 (m, 4H), 3.76 (m, 8H), 1.66 (s, 4H), 1.52–1.18 (m, 8H), 0.91 (s, 12H), 0.86 (t, *J* = 7.3 Hz, 24H).

^{13}C NMR (125 MHz, CD_2Cl_2) δ 159.54, 157.95, 156.31, 152.45, 151.39, 144.12, 142.83, 140.24, 136.85, 135.18, 129.52, 124.79, 122.21, 121.02, 116.68, 116.60, 115.09, 112.97, 112.88, 70.86, 64.16, 39.83, 37.79, 31.96, 30.89, 29.75, 29.49, 24.58, 24.22, 23.50, 23.08, 14.31, 14.22, 11.30.

2.1.2. Synthesis of Compound **3**

$POCl_3$ (1.66 g, 10.8 mmol) was slowly dropped into the mixture of compound **2** (1.8 g, 1.36 mmol) and DMF (0.88 g, 12 mmol) in toluene at −10° C and heated to 75 °C for eight hours. After removing the solvent, the mixture was purified through silica gel column chromatography (hexane/dichloromethane1:3). Compound **3** was obtained as an orange solid (1.5 g, 95%).

^{1}H NMR (300 MHz, CD_2Cl_2) δ 9.76 (s, 2H), 7.48 (s, 2H), 7.41 (s, 2H), 7.18 (t, *J* = 7.8 Hz, 4H), 6.96 (m, 4H), 6.90 (m, 4H), 6.81 (m, 4H), 3.78 (d, *J* = 5.7 Hz, 8H), 1.81–1.54 (m, 4H), 1.51–1.20 (m, 32H), 0.96 (s, 12H), 0.92–0.78 (m, 24H).

^{13}C NMR (125 MHz, CD_2Cl_2) δ 182.52, 161.53, 159.75, 158.49, 157.02, 151.54, 147.42, 145.99, 143.76, 143.51, 138.43, 135.78, 129.66, 121.44, 116.58, 115.98, 113.20, 70.92, 63.99, 46.73, 39.71, 30.86, 30.82, 29.44, 24.20, 24.17, 23.92, 23.45, 14.27, 11.25.

2.1.3. Synthesis of M-Me-ITIC Acceptors

INCN, INCN-Me, INCN-F, or INCN-Cl (0.82 mmol) and compound **3** (250 mg, 0.181 mmol) were dissolved in chloroform (30 mL), and pyridine (2 mL) was added. After string overnight at 65 °C, the mixture was poured into CH_3OH; the solid part was purified through silica-gel column chromatography (hexane/dichloromethane 1:5). m-Me-ITIC acceptors were obtained as blue solid.

m-Me-ITIC, (220 mg, 68%). ^{1}H NMR (300 MHz, CD_2Cl_2) δ 8.83 (s, 2H), 8.66–8.56 (m, 2H), 7.89–7.80 (m, 2H), 7.70 (dd, *J* = 5.3, 2.4 Hz, 4H), 7.52 (d, *J* = 16.1 Hz, 4H), 7.21 (t, *J* = 8.0 Hz, 4H), 7.02–6.88 (m, 8H), 6.83 (dd, *J* = 8.2, 2.4 Hz, 4H), 3.79 (d, *J* = 5.7 Hz, 8H), 1.66 (m, 4H), 1.49–1.20 (m, 32H), 1.00 (s, 12H), 0.87 (m, 24H). ^{13}C NMR (126 MHz, $CDCl_3$) δ 188.67, 161.03, 160.73, 159.41, 157.49, 151.68, 142.74, 140.09, 136.89, 136.21, 134.73, 134.02, 129.49, 125.11, 123.38, 121.22, 116.55, 116.35, 115.45, 115.32, 112.95, 70.72, 66.92, 63.67, 46.35, 39.36, 30.58, 30.55, 29.82, 29.17, 29.14, 24.07, 23.91, 23.88, 23.14, 14.22, 11.19, 11.17. MS (MALDI-TOF) calcd. For $C_{112}H_{110}N_4O_6S_4$, 1734.7308; found, 1734.7863.

m-Me-ITIC-Me, (210 mg, 66%). ^{1}H NMR (300 MHz, CD_2Cl_2) δ 8.80 (s, 2H), 8.50 (d, *J* = 8.1 Hz, 0.6H), 8.43 (s, 1.4H), 7.74 (d, *J* = 7.6 Hz, 1.4H), 7.66 (s, 0.6H), 7.59–7.44 (m, 6H), 7.20 (t, *J* = 8.0 Hz, 4H), 6.99–6.87 (m, 8H), 6.82 (dd, *J* = 8.3, 2.3 Hz, 4H), 3.79 (d, *J* = 5.7 Hz, 8H), 2.52 (d, *J* = 3.6 Hz, 6H), 1.66 (p, *J* = 6.1 Hz, 4H), 1.47–1.18 (m, 32H), 0.99 (s, 12H), 0.92–0.80 (m, 24H). ^{13}C NMR (125 MHz, $CDCl_3$) δ 188.79, 188.47, 160.83, 159.40, 157.41, 151.61, 151.34, 146.23, 145.70, 142.80, 140.49, 137.70, 137.27, 136.53, 136.17, 135.59, 134.99, 134.75, 129.47, 125.55, 125.07, 123.78, 123.31, 121.23, 116.55, 116.30, 115.50, 115.38, 112.95, 70.71, 66.72, 66.27, 63.67, 46.34, 39.36, 30.59, 30.56, 29.17, 29.14, 24.07, 23.91, 23.89, 23.15, 22.63, 22.15, 14.22, 11.20, 11.17. MS (MALDI-TOF) calcd. For $C_{114}H_{114}N_4O_6S_4$, 1762.7621; found, 1762.7922.

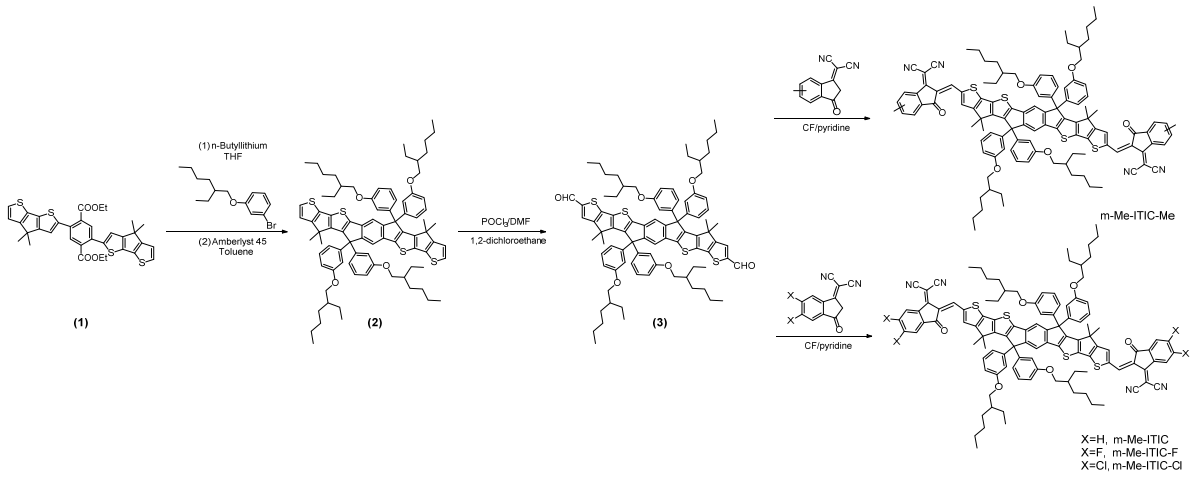
m-Me-ITIC-F, (250 mg, 78%). ^{1}H NMR (300 MHz, CD_2Cl_2) δ 8.81 (s, 2H), 8.46 (dd, *J* = 10.3, 6.5 Hz, 2H), 7.66–7.47 (m, 6H), 7.20 (t, *J* = 8.0 Hz, 4H), 6.98–6.87 (m, 8H), 6.82 (dd, *J* = 8.2, 2.4 Hz, 4H), 3.78 (d, *J* = 5.7 Hz, 8H), 1.64 (m, 4H), 1.52–1.20 (m, 32H), 0.99 (s, 12H), 0.95–0.80 (m, 24H).^{13}C NMR (125 MHz, $CDCl_3$) δ 186.16, 162.93, 161.70, 159.43, 158.49, 157.94, 157.69, 155.23, 155.12, 153.16, 153.06, 153.03, 152.61, 151.76, 142.59, 139.26, 137.63, 137.21, 136.55, 136.33, 134.41, 134.36, 129.50, 121.17, 118.64, 116.58, 116.53, 115.02, 114.94, 114.87, 114.69, 112.96, 112.34, 112.20, 70.72, 67.16, 63.70, 46.37, 39.35, 30.56, 30.53, 29.16, 29.13, 24.01, 23.89, 23.87, 23.13, 14.21, 11.18, 11.15.MS (MALDI-TOF) calcd. For $C_{112}H_{106}F_4N_4O_6S_4$, 1806.6931; found, 1806.7775.

m-Me-ITIC-Cl, (250 mg, 74%). ^{1}H NMR (300 MHz, CD_2Cl_2) δ 8.81 (s, 2H), 8.66 (s, 2H), 7.75 (d, *J* = 2.0 Hz, 2H), 7.54 (d, *J* = 3.1 Hz, 4H), 7.19 (t, *J* = 8.0 Hz, 4H), 6.96–6.88 (m, 8H),6.84–6.76 (m, 4H), δ 3.77 (d, *J* = 5.7 Hz, 8H),1.63 (m, 4H), 1.48–1.19 (m, 32H), 0.99 (s, 12H), 0.86 (m, 24H).^{13}C NMR (125 MHz, $CDCl_3$) δ 186.11, 163.07, 161.94, 159.41, 158.56, 158.29, 157.78, 153.05, 151.80, 142.55, 139.66, 139.42, 138.91, 138.70, 137.95, 137.33, 136.40, 135.96, 129.49, 126.58, 124.67, 121.18, 118.54, 116.72, 116.53, 115.12, 114.94, 112.92, 70.75, 67.02, 63.71, 46.35, 39.34, 30.55, 30.52, 29.16, 29.12, 24.00, 23.87, 23.14, 14.22, 11.19, 11.16. MS (MALDI-TOF) calcd. For $C_{112}H_{106}Cl_4N_4O_6S_4$, 1870.5749; found, 1870.6914.

3. Result and Discussion

The synthetic scheme of m-Me-ITIC series was presented in Scheme 1. We treated compound **1** with freshly prepared (3-((2-ethylhexyl)oxy)phenyl)lithium-yielded diol, then intramolecular Friedel–Crafts cyclization to was carried out to furnish compound **2** (IT). This IT was reacted with $POCl_3$ and dimethylformamide to yield carbaldehyde, which was then capped with various IC groups by the Knoevenagel condensation reaction to generate the desired compound. Each of the new acceptors was characterized by NMR, and mass spectrometry (Figures S1–S6 in Supporting Information). The resulting acceptors showed good solubility at room temperature in common solvent.

Thermogravimetric analysis (TGA) and differential scanning calorimetry (DSC) was carried out to investigate the thermal stability of the m-Me-ITIC acceptors (Figures S7 and S8 in Supporting Information). All four acceptors have decomposition temperatures (Td) > 330 °C (5% weight loss), indicating m-Me-ITIC series have good thermal stability. Differential scanning calorimetry revealed that m-Me-ITIC-Cl undergoes an endothermic melting transition at 144 °C. This thermal transition implies that m-Me-ITIC-Cl has a greater tendency to crystallize than the other derivatives because of end group differences.



Scheme 1. Synthetic scheme for m-Me-ITIC series acceptors.

The ultraviolet–visible absorption spectra and corresponding data of the m-Me-ITIC series in chloroform and thin film are shown in Figure 1b,c and Table 1. The entire series exhibited large red-shifts > 100 nm compared with ITIC-ethylhexyl oxy (OEH), which was composed of thienothiophene instead of CPDT due to the extended conjugation. Furthermore, measurement of ultraviolet–visible spectra in solution revealed that λ_{max} exhibited greater red-shifts with increasing electron acceptor ability: m-Me-ITIC-Me (λ_{max}: 756 nm) < m-ITIC (760 nm) < m-ITIC-F (775 nm) < m-ITIC-Cl (790 nm). In thin film, a broader spectrum and redshifted maximum absorption were observed for m-Me-ITIC acceptors; the absorption maximum of m-Me-ITIC-Cl was shifted by nearly 16 nm compared with m-Me-ITIC-F, suggesting that stronger π–π interactions occur in thin film. We conducted our electrochemical study of the m-Me-ITIC series using cyclic voltammetry for energy level measurement (Figure S9 in Supporting Information). Owing to the electronegative nature of INIC group, the LUMO energy levels of the corresponding NFAs decreased from −4.19 and −4.20 eV for m-Me-ITIC-M and m-Me-ITIC, respectively, to −4.29 eV for m-Me-ITIC-F and −4.35 eV for m-Me-ITIC-Cl.

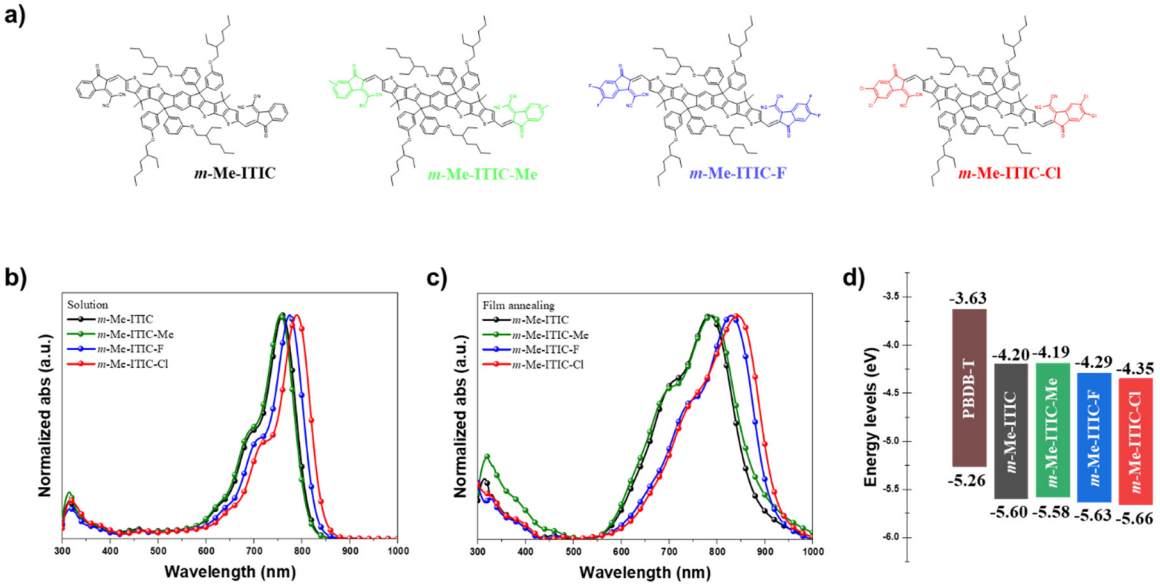


Figure 1. (**a**) Chemical structures of the m-Me-ITIC series acceptors. (**b**) Absorption spectra of the m-Me-ITIC series in chloroform solution and (**c**) as thin films. (**d**) Schematic illustration of HOMO/LUMO energy levels of donor, m-Me-ITIC, m-Me-ITIC-Me, m-Me-ITIC-F, and m-Me-ITIC-Cl.

Table 1. Optical and Electrochemical Properties of acceptors.

Materials	$HOMO^{cv}$ (eV)	$LUMO^{opt}$ (eV)	$\lambda_{max}{}^{sol}$ (nm)	$\lambda_{max}{}^{film}$ (nm)	λ_{onset} (nm)	ε (mol^{-1} cm^{-1} L)	$E_g{}^{opt}$ (eV)
m-Me-ITIC	−5.60	−4.20	760	788	885	2.04×10^5	1.40
m-Me-ITIC-Me	−5.58	−4.19	756	789	890	1.88×10^5	1.39
m-Me-ITIC-F	−5.63	−4.29	775	830	920	1.83×10^5	1.35
m-Me-ITIC-Cl	−5.66	−4.35	790	846	930	1.72×10^5	1.33

To demonstrate the photovoltaic performances of m-Me-ITIC acceptors, we fabricated organic photovoltaic (OPV) devices by blending m-Me-ITIC acceptors with PBDB-T polymer donor using an inverted structure with glass/tin-doped indium oxide/ZnO/BHJ/MoO_x/Ag. Current density–voltage (*J*–*V*) characteristics of the optimized devices with the m-Me-ITIC acceptors was measured under simulated AM1.5 G with an intensity of 100 mW/cm^2, the results are shown in Figure 2a and the device data are summarized in Table 2. To verify the measurement accuracy, we crosschecked the external quantum efficiency spectra with the *J*–*V* characteristics (Figure 2b and Table 2). We summarize the device optimization data (e.g., thermal annealing, donor/acceptor blending ratio, and processing additive of each OPV device) (Tables S1–S6 in Supporting Information). Thus, the efficiency-optimized devices made from m-Me-ITIC, m-Me-ITIC-Me, m-Me-ITIC-F, and m-Me-ITIC-Cl demonstrated PCE values of 5.9%, 3.6%, 11.8%, and 10.8%, respectively.

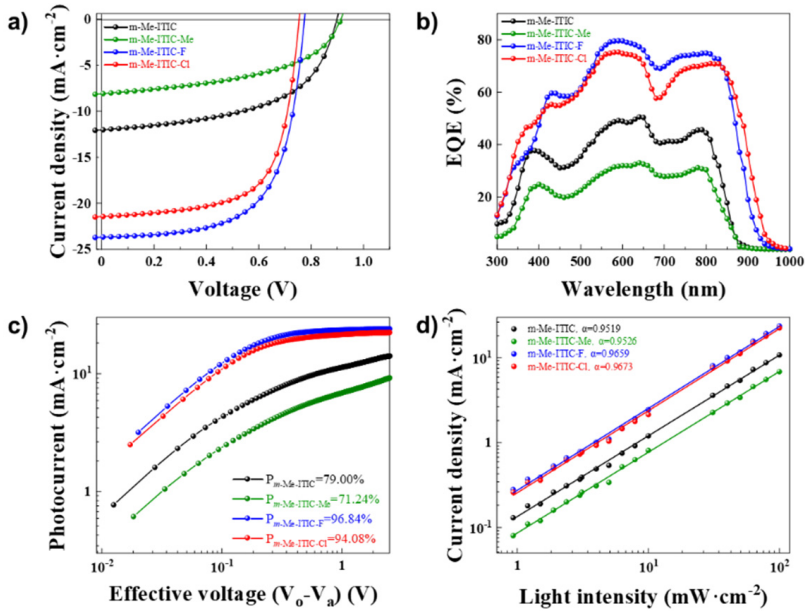


Figure 2. (**a**) *J*–*V* characteristics, (**b**) EQE spectra, (**c**) Photocurrent versus effective voltage, and (**d**) Current density versus light intensity of OPV cells based on PBDB-T: m-Me-ITIC, PBDB-T: m-Me-ITIC-Me, PBDB-T: m-Me-ITIC-F, and PBDB-T: m-Me-ITIC-Cl.

To further understand the collection behaviors and charge dissociation of the four fabricated OPV cells, the photocurrent density (J_{ph}) on the effective voltage (V_{eff}) was investigated, the results are presented in Figure 2c. V_{eff} was determined using the following equation: $V_{eff} = V_0 - V_a$, where V_0 indicates the voltage when illuminated with a current density (J_L) identical to the dark current density (J_D), and V_a indicates the applied voltage. J_{ph} was determined using the following equation: $J_{ph} = J_L - J_D$ [52,53]. Each of the OPV cells was biased from −2.0 to 1.0 V to demonstrate the exciton dissociation process; the saturation current density (J_{sat}) was verified for a V_{eff} of 2.5 V. The J_{sat} values measured for m-Me-ITIC, m-Me-ITIC-Me, m-Me-ITIC-F, and m-Me-ITIC-Cl were 14.12, 9.20, 24.00, and 22.40 mA·cm^{-2}. We divided the normalized J_{ph} by J_{sat} to calculate P(E,T) to demonstrate

the exciton dissociation as well as charge collection properties. The P(E,T) values calculated were 79.00%, 71.24%, 96.84%, and 94.08%, respectively, indicating that OPV cells using novel NFAs with the halogen end groups fluorine or chlorine demonstrate better charge collection and faster exciton dissociation than OPV cells using the other two NFAs [54].

Table 2. The optimized photovoltaic performances of the OPV cells under simulated illumination of AM 1.5 G (100 mW·cm^{-2}).

Photoactive Materials	V_{OC} (V)	J_{SC} (mA·cm^{-2})	EQE (mA·cm^{-2})	FF	PCE_{best}/PCE_{avg} [a] (%)
[b] PBDB-T:m-Me-ITIC	0.90 (0.89 ± 0.01)	12.00 (9.97 ± 1.22)	12.64	0.54 (0.54 ± 0.05)	5.90 (4.79 ± 0.41)
[b] PBDB-T:m-Me-ITIC-Me	0.92 (0.92 ± 0.01)	8.10 (6.90 ± 0.80)	8.30	0.49 (0.48 ± 0.02)	3.60 (3.05 ± 0.33)
[c] PBDB-T:m-Me-ITIC-F	0.78 (0.78 ± 0.00)	22.80 (21.04 ± 1.38)	22.80	0.67 (0.68 ± 0.02)	11.80 (11.07 ± 0.50)
[d] PBDB-T:m-Me-ITIC-Cl	0.75 (0.75 ± 0.00)	21.50 (18.64 ± 1.91)	22.19	0.67 (0.69 ± 0.02)	10.80 (9.74 ± 0.79)

[a] The Average PCE values are achieved from 10 devices. [b] The blending ratio of the device is 1:1.2 and without additive. [c] The blending ratio of the device is 1:1 and with 0.5 vol% 1-chloronaphthalene. [d] The blending ratio of the device is 1:1 and with 1.5 vol% 1,8-diiodooctane.

To investigate the charge transport behaviors, we analyzed the J_{sc} value of each cell by varying the irradiated light intensity (P_{light}) from 0.93 to 100 mW·cm^{-2}, as shown in Figure 2d. The relationship between J_{sc} and P_{light} can be described as $J_{sc} \propto P_{light}^{\alpha}$, where α is an exponential factor. A value for α close to unity indicates weak bimolecular recombination. As the value of α decreases, severe bimolecular recombination occurs [55]. The α-values of m-Me-ITIC-F blend and m-Me-ITIC-Cl blend was calculated as 0.9659 and 0.9673, which is higher than the α-values of m-Me-ITIC blend and m-Me-ITIC-Me blend (0.9519 and 0.9526, respectively). Because bimolecular recombination induces partial charge carrier losses [56], we presume that minimizing bimolecular recombination will help to increase the J_{sc} value and fill factor of the OPV devices based on NFAs with halogen end groups (m-Me-ITIC-F and m-Me-ITIC-Cl).

To study the charge transport properties of the OSCs further, the devices' electron and hole mobilities were evaluated by the space charge limited current (SCLC) method (Figure S10 and Table S7 in Supporting Information). The electron mobility and hole mobility were measured with the device structure of ITO/ZnO/Active layer/BCP/Al and ITO/PEDOT:PSS/Active layer/MoOx/Ag, respectively. The calculated hole/electron (μ_h/μ_e) of the PBDB-T:m-Me-ITIC, PBDB-T:m-Me-ITIC-Me, PBDB-T:m-Me-ITIC-F, and PBDB-T:m-Me-ITIC-Cl devices were $4.38 \times 10^{-4}/5.62 \times 10^{-4}$, $4.46 \times 10^{-4}/5.53 \times 10^{-4}$, $6.55 \times 10^{-4}/6.47 \times 10^{-4}$, and $5.17 \times 10^{-4}/5.61 \times 10^{-4}$ cm^2 V^{-1} s^{-1}, which is equivalent to μ_h/μ_e ratios of 0.78, 0.81, 1.01, and 0.92, respectively. The PBDB-T:m-Me-ITIC-F and PBDB-T:m-Me-ITIC-Cl devices showed higher and more balanced charge transport than PBDB-T:m-Me-ITIC, PBDB-T:m-Me-ITIC-Me, which could reduce charge recombination, thus contributing to the enhanced J_{sc} and fill factor.

Atomic force microscopy (AFM) was employed to investigate the morphologies of the m-Me-ITIC-, m-Me-ITIC-Me-, m-Me-ITIC-F-, and m-Me-ITIC-Cl-based BHJ films, the detail was shown in Figure 3. The root-mean-square surface roughness (RMS) values were higher for all BHJ blend films than for the novel NFA films. The RMS values of m-Me-ITIC and m-Me-ITIC-Me blend were <1 nm (0.97 and 0.83 nm, respectively), while the values of m-Me-ITIC-F and m-Me-ITIC-Cl blend were close to 1.5 nm. The exciton dissociation, charge transport, and charge collection ability of OPVs can be determined by BHJ film morphology. Favorable phase separation between donor and acceptor in m-Me-ITIC-F blend and m-Me-ITIC-Cl blend may have produced a slightly rougher surface, increasing

the efficiency of these OPV cells [57,58]. These results consistently show the effects of the halogen end group on the novel NFAs.

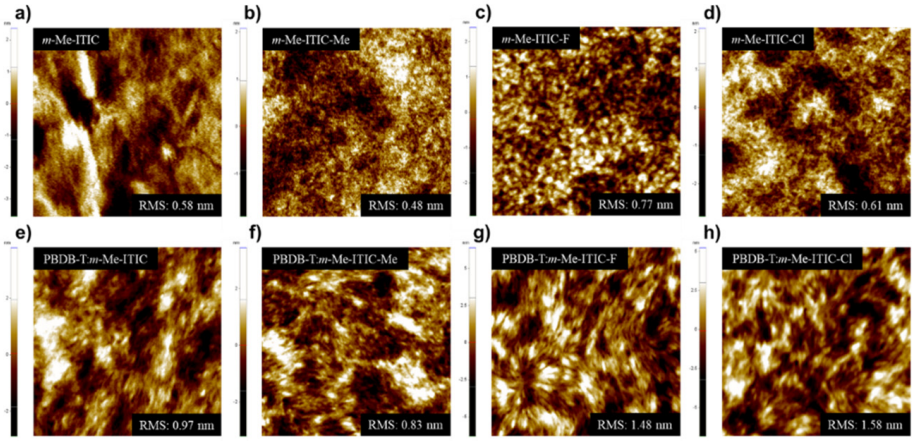


Figure 3. Atomic force microscopy (AFM) height images of (**a**) m-Me-ITIC, (**b**) m-Me-ITIC-Me, (**c**) m-Me-ITIC-F, (**d**) m-Me-ITIC-Cl, (**e**) PBDB-T: m-Me-ITIC, (**f**) PBDB-T: m-Me-ITIC-Me, (**g**) PBDB-T: m-Me-ITIC-F, and (**h**) PBDB-T: m-Me-ITIC-Cl.

To confirm the crystallinity of the fabricated BHJ films based on novel NFAs, X-ray diffraction was performed. Figure 4a shows the X-ray diffraction patterns of neat acceptor films. 2θ diffraction peaks are located at 5.22°, 4.20°, 3.54°, and 3.39°, respectively; these values correspond to d-spacings of 16.91, 21.02, 24.94, and 26.02 Å, respectively. Notably, the diffraction peaks of the m-Me-ITIC-F and m-Me-ITIC-Cl films are clear and distinct. As shown in Figure 4b, the 2θ diffraction peaks of m-Me-ITIC, m-Me-ITIC-F, and m-Me-ITIC-Cl BHJ blend films are located at 3.20°, 3.61°, and 3.66°, respectively; these values correspond to d-spacings of 27.61, 24.46, and 24.09 Å, respectively. When the novel NFAs were mixed with the donor to produce blended BHJ films, the crystallinity of the PBDB-T:m-Me-ITIC-Me film almost disappeared compared to pristine m-Me-ITIC-Me. Although the peaks of the other BHJ films remained visible, lamellar distances were shorter for m-Me-ITIC-F blend and m-Me-ITIC-Cl blend than m-Me-ITIC blend. This might be caused by strong intermolecular interactions through the highly electronegative halogen atoms used as end groups, which could induce greater molecular polarization [59]. This might be consistent evidence for highly efficient OPV cells based on m-Me-ITIC-F and m-Me-ITIC-Cl.

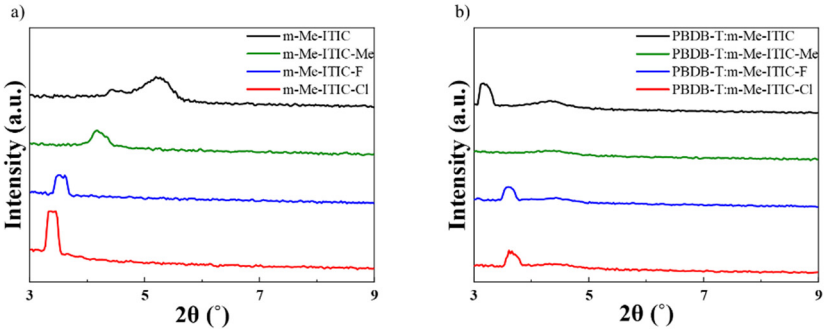


Figure 4. XRD patterns of (**a**) m-Me-ITIC, m-Me-ITIC-Me, m-Me-ITIC-F, and m-Me-ITIC-Cl films, (**b**) PBDB-T: m-Me-ITIC, PBDB-T: m-Me-ITIC-Me, PBDB-T: m-Me-ITIC-F, PBDB-T: m-Me-ITIC-Cl blend films. List of Tables.

4. Conclusions

We designed and synthesized a 9-heterocyclic ring acceptor, m-Me-ITIC, with different end groups by substituting the outward thienothiophene moieties with CPDT at indacenodithiophene. The developed m-Me-ITIC, m-Me-ITIC-Me, m-Me-ITIC-F, and m-Me-ITIC-Cl

showed long-wavelength absorption at approximately 756–790 nm in solution because of the symmetric, planar, and extended conjugated CPDT donor. The m-Me-ITIC-based acceptors were developed into polymer solar cells that contained benzodithiophene-based donor polymers. The devices optimized for efficiency demonstrated PCEs of 5.9%, 3.6%, 11.8%, and 10.8% using m-Me-ITIC, m-Me-ITIC-Me, m-Me-ITIC-F, and m-Me-ITIC-Cl, respectively. Analyses of the charge dissociation and collection behaviors of the four fabricated OPV cells found that the new NFAs with halogen end groups showed salient bimolecular recombination dynamics. The BHJ film morphology for exciton dissociation, charge transport, and charge collection ability of the OPVs showed favorable phase separation in m-Me-ITIC-F blend and m-Me-ITIC-Cl blend. The shorter lamellar distances of these two materials, caused by strong intermolecular interactions through the highly electronegative halogen atoms, could induce greater molecular polarization. This may also be consistent evidence for highly efficient OPV cells based on m-Me-ITIC-F and m-Me-ITIC-Cl.

Supplementary Materials: The following supporting information can be downloaded at: https://www.mdpi.com/article/10.3390/molecules27217615/s1, Figure S1: ^{1}H-NMR and ^{13}C-NMR of compound **2**; Figure S2: ^{1}H-NMR and ^{13}C-NMR of compound **3**; Figure S3: ^{1}H-NMR and ^{13}C-NMR of m-Me-ITIC; Figure S4: ^{1}H-NMR and ^{13}C-NMR of compound m-Me-ITIC-Me; Figure S5: ^{1}H-NMR and ^{13}C-NMR of m-Me-ITIC-F; Figure S6: ^{1}H-NMR and ^{13}C-NMR of m-Me-ITIC-Cl; Figure S7: TGA curves of (a) m-Me-ITIC, (b)m-Me-ITIC-Me, (c) m-Me-ITIC-F, and (d) m-Me-ITIC-Cl with a heating rate of 10 °C/min; Figure S8: DSC thermograms of m-Me-ITIC-X (a) heat-only thermograms and (b) cool-only thermograms; Figure S9: CV curves measured from Chloroform solution of m-Me-ITIC-Xs; Figure S10: SCLC measurements of hole- and electron-only devices. *J*–*V* characteristics of (a) hole-only devices and (b) electron-only devices based on PBDB-T and the acceptors blend films; Table S1: The photovoltaic parameters of the OPVs based on PBDB-T:m-Me-ITIC, PBDB-T:m-Me-ITIC-Me, PBDB-T:m-Me-ITIC-F, and PBDB-T:m-Me-ITIC-Cl with or without thermal annealing for 20 min under the illumination of AM 1.5G, 100 mW·cm^{-2}; Table S2: The photovoltaic parameters of the OPVs based on PBDB-T:m-Me-ITIC, PBDB-T:m-Me-ITIC-Me, m-Me-ITIC-F, and m-Me-ITIC-Cl with different donor:acceptor blend ratios under the illumination of AM 1.5G, 100 mW·cm^{-2}; Table S3: The optimized photovoltaic performances of the OSCs based on PBDB-T:m-Me-ITIC with different additives under the illumination of AM 1.5G, 100 mW·cm^{-2}; Table S4: The optimized photovoltaic performances of the OSCs based on PBDB-T:m-Me-ITIC-Me with different additives under the illumination of AM 1.5G, 100 mW·cm^{-2}; Table S5: The optimized photovoltaic performances of the OSCs based on PBDB-T:m-Me-ITIC-F with different additives under the illumination of AM 1.5G, 100 mW·cm^{-2}; Table S6: The optimized photovoltaic performances of the OSCs based on PBDB-T:m-Me-ITIC-Cl with different additives under the illumination of AM 1.5G, 100 mW·cm^{-2}; Table S7: Hole and electron mobilities of the devices based on PBDB-T and the acceptors blend films.

Author Contributions: C.S. and S.L. contributed equally to this work. Conceptualization: C.S., S.L., K.L.; Methodology: C.S., S.L.; Investigation: C.S., S.L., S.J.; Formal analysis: C.S., S.L., C.C., S.J., J.O., J.-H.K., J.K., H.E.B.; Data curation: H.K., H.H.C.; Validation: H.K.; Visualization: S.L., J.K.; Writing—original draft preparation: C.S., S.L., J.K., S.-Y.J.; Writing—review and editing: S.-Y.J., H.H.C.; Supervision: S.-Y.J., K.L., Y.-H.K.; Project administration: S.-Y.J., H.H.C., K.L., Y.-H.K.; Funding acquisition: K.L., Y.-H.K. All authors have read and agreed to the published version of the manuscript.

Funding: National Research Foundation (NRF) funded by the Ministry of Science, ICT & Future Planning, Republic of Korea (NRF 2021R1A2B5B03086367, NRF 2022M3J7A1062940, NRF 2017K1A1A2013153, NRF 2020M1A2A2080748, NRF 2020R1A2C3003653, and NRF 2020R1A6A03038697) and GIST Research Institute (GRI) grant.

Institutional Review Board Statement: Not applicable.

Informed Consent Statement: Not applicable.

Data Availability Statement: Not applicable.

Acknowledgments: This research was supported by National Research Foundation (NRF) funded by the Ministry of Science, ICT & Future Planning (NRF 2021R1A2B5B03086367, NRF 2022M3J7A1062940, NRF

2017K1A1A2013153, NRF 2020M1A2A2080748, NRF 2020R1A2C3003653, and NRF 2020R1A6A03038697) and This work was supported by the GIST Research Institute (GRI) grant funded by the GIST in 2022.

Conflicts of Interest: The authors declare that they have no known competing financial interests or personal relationships that could have appeared to influence the work reported in this paper.

References

1. Yan, C.; Barlow, S.; Wang, Z.; Yan, H.; Jen, A.K.Y.; Marder, S.R.; Zhan, X. NFAsfor organic solar cells. *Nat. Rev. Mater.* **2018**, *3*, 18003. [CrossRef]
2. Hou, J.; Inganäs, O.; Friend, R.H.; Gao, F. Organic solar cells based on non-fullerene acceptors. *Nat. Mater.* **2018**, *17*, 119–128. [CrossRef] [PubMed]
3. Zhang, Y.; Kan, B.; Sun, Y.; Wang, Y.; Xia, R.; Ke, X.; Yi, Y.-Q.; Li, C.; Yip, H.-L.; Wan, X.; et al. Nonfullerene Tandem Organic Solar Cells with High Performance of 14.11%. *Adv. Mater.* **2018**, *30*, e1707508. [CrossRef] [PubMed]
4. Sun, J.; Ma, X.; Zhang, Z.; Yu, J.; Zhou, J.; Yin, X.; Yang, L.; Geng, R.; Zhu, R.; Zhang, F.; et al. Dithieno[3,2-*b*:2′,3′-*d*]pyrrol Fused Nonfullerene Acceptors Enabling Over 13% Efficiency for Organic Solar Cells. *Adv. Mater.* **2018**, *30*, e1707150. [CrossRef] [PubMed]
5. Zhang, J.; Tan, H.S.; Guo, X.; Facchetti, A.; Yan, H. Material insights and challenges for non-fullerene organic solar cells based on small molecular acceptors. *Nat. Energy* **2018**, *3*, 720–731. [CrossRef]
6. Kim, G.; Sun, C.; Lee, D.; Choi, G.; Park, J.S.; Seo, S.; Lee, S.; Choi, D.; Kwon, S.; Cho, S.; et al. Effect of the Selective Halogenation of Small Molecule Acceptors on the Blend Morphology and Voltage Loss of High-Performance Solar Cells. *Adv. Funct. Mater.* **2022**, *32*, 2201150. [CrossRef]
7. Kim, C.; Chen, S.; Park, J.S.; Kim, G.-U.; Kang, H.; Lee, S.; Phan, T.N.-L.; Kwon, S.-K.; Kim, Y.-H.; Kim, B.J. Green solvent-processed, high-performance organic solar cells achieved by outer side-chain selection of selenophene-incorporated Y-series acceptors. *J. Mater. Chem. A* **2021**, *9*, 24622–24630. [CrossRef]
8. Labanti, C.; Sung, M.J.; Luke, J.; Kwon, S.; Kumar, R.; Hong, J.; Kim, J.; Bakulin, A.A.; Kwon, S.-K.; Kim, Y.-H.; et al. Selenium-Substituted Non-Fullerene Acceptors: A Route to Superior Operational Stability for Organic Bulk Heterojunction Solar Cells. *ACS Nano* **2021**, *15*, 7700–7712. [CrossRef]
9. Ouyang, X.; Peng, R.; Ai, L.; Zhang, X.; Ge, Z. Efficient polymer solar cells employing a non-conjugated small-molecule electrolyte. *Nat. Photon.* **2015**, *9*, 520–524. [CrossRef]
10. Zhang, K.; Gao, K.; Xia, R.; Wu, Z.; Sun, C.; Cao, J.; Qian, L.; Li, W.; Liu, S.; Huang, F.; et al. High-Performance Polymer Tandem Solar Cells Employing a New n-Type Conjugated Polymer as an Interconnecting Layer. *Adv. Mater.* **2016**, *28*, 4817–4823. [CrossRef]
11. Xu, X.; Li, Z.; Wang, Z.; Li, K.; Feng, K.; Peng, Q. 10.20% Efficiency polymer solar cells via employing bilaterally hole-cascade diazaphenanthrobisthiadiazole polymer donors and electron-cascade indene-C70 bisadduct acceptor. *Nano Energy* **2016**, *25*, 170–183. [CrossRef]
12. Zhao, J.; Li, Y.; Yang, G.; Jiang, K.; Lin, H.; Ade, H.; Ma, W.; Yan, H. Efficient organic solar cells processed from hydrocarbon solvents. *Nat. Energy* **2016**, *1*, 15027. [CrossRef]
13. Liu, T.; Troisi, A. What Makes Fullerene Acceptors Special as Electron Acceptors in Organic Solar Cells and How to Replace Them. *Adv. Mater.* **2012**, *25*, 1038–1041. [CrossRef] [PubMed]
14. He, Y.; Li, Y. Fullerene derivative acceptors for high performance polymer solar cells. *Phys. Chem. Chem. Phys.* **2010**, *13*, 1970–1983. [CrossRef] [PubMed]
15. Zhao, J.; Li, Y.; Lin, H.; Liu, Y.; Jiang, K.; Mu, C.; Ma, T.; Lai, J.Y.L.; Hu, H.; Yu, D.; et al. High-efficiency non-fullerene organic solar cells enabled by a difluorobenzothiadiazole-based donor polymer combined with a properly matched small molecule acceptor. *Energy Environ. Sci.* **2014**, *8*, 520–525. [CrossRef]
16. Shi, H.; Fu, W.; Shi, M.; Ling, J.; Chen, H. A solution-processable bipolar diketopyrrolopyrrole molecule used as both electron donor and acceptor for efficient organic solar cells. *J. Mater. Chem. A* **2014**, *3*, 1902–1905. [CrossRef]
17. Bin, H.; Yao, J.; Yang, Y.; Angunawela, I.; Sun, C.; Gao, L.; Ye, L.; Qiu, B.; Xue, L.; Zhu, C.; et al. High-Efficiency All-Small-Molecule Organic Solar Cells Based on an Organic Molecule Donor with Alkylsilyl-Thienyl Conjugated Side Chains. *Adv. Mater.* **2018**, *30*, e1706361. [CrossRef]
18. Huang, J.; Carpenter, J.H.; Li, C.-Z.; Yu, J.-S.; Ade, H.; Jen, A.K.-Y. Highly Efficient Organic Solar Cells with Improved Vertical Donor-Acceptor Compositional Gradient Via an Inverted Off-Center Spinning Method. *Adv. Mater.* **2015**, *28*, 967–974. [CrossRef]
19. Li, Z.; Yang, D.; Zhao, X.; Zhang, T.; Zhang, J.; Yang, X. Achieving an Efficiency Exceeding 10% for Fullerene-based Polymer Solar Cells Employing a Thick Active Layer via Tuning Molecular Weight. *Adv. Funct. Mater.* **2017**, *28*, 1705257. [CrossRef]
20. Li, W.; Cai, J.; Cai, F.; Yan, Y.; Yi, H.; Gurney, R.S.; Liu, D.; Iraqi, A.; Wang, T. Achieving over 11% power conversion efficiency in PffBT4T-2OD-based ternary polymer solar cells with enhanced open-circuit-voltage and suppressed charge recombination. *Nano Energy* **2018**, *44*, 155–163. [CrossRef]
21. Yuan, J.; Qiu, L.; Zhang, Z.-G.; Li, Y.; Chen, Y.; Zou, Y. Tetrafluoroquinoxaline based polymers for non-fullerene polymer solar cells with efficiency over 9%. *Nano Energy* **2016**, *30*, 312–320. [CrossRef]

22. Yi, J.; Wang, Y.; Luo, Q.; Lin, Y.; Tan, H.; Wang, H.; Ma, C.-Q. A 9,9′-spirobi[9H-fluorene]-cored perylenediimide derivative and its application in organic solar cells as a non-fullerene acceptor. *Chem. Commun.* **2015**, *52*, 1649–1652. [CrossRef] [PubMed]
23. Li, S.; Zhang, Z.; Shi, M.; Li, C.-Z.; Chen, H. Molecular electron acceptors for efficient fullerene-free organic solar cells. *Phys. Chem. Chem. Phys.* **2016**, *19*, 3440–3458. [CrossRef] [PubMed]
24. Yang, L.; Zhang, S.; He, C.; Zhang, J.; Yao, H.; Yang, Y.; Zhang, Y.; Zhao, W.; Hou, J. New Wide Band Gap Donor for Efficient Fullerene-Free All-Small-Molecule Organic Solar Cells. *J. Am. Chem. Soc.* **2017**, *139*, 1958–1966. [CrossRef] [PubMed]
25. Mao, Y.; Guo, C.; Li, D.; Li, W.; Du, B.; Chen, M.; Wang, Y.; Liu, D.; Wang, T. Molecular Ordering and Performance of Ternary Nonfullerene Organic Solar Cells via Bar-Coating in Air with an Efficiency over 13%. *ACS Appl. Mater. Interfaces* **2019**, *11*, 35827–35834. [CrossRef] [PubMed]
26. Li, G.; Wang, S.; Liu, T.; Hao, P.; Liu, Z.; Li, F.; Yang, L.-M.; Zhang, Y.; Li, D.; Yang, S.; et al. Non-fullerene acceptor engineering with three-dimensional thiophene/selenophene-annulated perylene diimides for high performance polymer solar cells. *J. Mater. Chem. C* **2018**, *6*, 12601–12607. [CrossRef]
27. Yao, C.; Liu, B.; Zhu, Y.; Hong, L.; Miao, J.; Hou, J.; He, F.; Meng, H. Highly fluorescent anthracene derivative as a non-fullerene acceptor in OSCs with small non-radiative energy loss of 0.22 eV and high PCEs of over 13%. *J. Mater. Chem. A* **2019**, *7*, 10212–10216. [CrossRef]
28. Lee, S.; Park, K.H.; Lee, J.; Back, H.; Sung, M.J.; Lee, J.; Kim, J.; Kim, H.; Kim, Y.; Kwon, S.; et al. Achieving Thickness-Insensitive Morphology of the Photoactive Layer for Printable Organic Photovoltaic Cells via Side Chain Engineering in Nonfullerene Acceptors. *Adv. Energy Mater.* **2019**, *9*, 1900044. [CrossRef]
29. Lin, Y.; Zhan, X. Designing Efficient Non-Fullerene Acceptors by Tailoring Extended Fused-Rings with Electron-Deficient Groups. *Adv. Energy Mater.* **2015**, *5*, 1501063. [CrossRef]
30. Wadsworth, A.; Moser, M.; Marks, A.; Little, M.S.; Gasparini, N.; Brabec, C.J.; Baran, D.; McCulloch, I. Critical review of the molecular design progress in non-fullerene electron acceptors towards commercially viable organic solar cells. *Chem. Soc. Rev.* **2018**, *48*, 1596–1625. [CrossRef]
31. Shi, J.; Isakova, A.; Abudulimu, A.; Berg, M.V.D.; Kwon, O.K.; Meixner, A.J.; Park, S.Y.; Zhang, D.; Gierschner, J.; Lüer, L. Designing high performance all-small-molecule solar cells with non-fullerene acceptors: Comprehensive studies on photoexcitation dynamics and charge separation kinetics. *Energy Environ. Sci.* **2017**, *11*, 211–220. [CrossRef]
32. Jia, J.; Liu, G.; Jia, T.; Wang, Z.; Lin, K.; Li, Y.; Huang, F.; Cao, Y. Fused nonacyclic electron acceptors with additional alkyl side chains for efficient polymer solar cells. *Org. Electron.* **2019**, *68*, 151–158. [CrossRef]
33. Gao, W.; Liu, T.; Luo, Z.; Zhang, L.; Ming, R.; Zhong, C.; Ma, W.; Yan, H.; Yang, C. Regulating exciton bonding energy and bulk heterojunction morphology in organic solar cells via methyl-functionalized non-fullerene acceptors. *J. Mater. Chem. A* **2019**, *7*, 6809–6817. [CrossRef]
34. Song, J.; Li, C.; Ye, L.; Koh, C.; Cai, Y.; Wei, D.; Woo, H.Y.; Sun, Y. Extension of indacenodithiophene backbone conjugation enables efficient asymmetric A–D–A type non-fullerene acceptors. *J. Mater. Chem. A* **2018**, *6*, 18847–18852. [CrossRef]
35. Li, Y.; Zhong, L.; Gautam, B.; Bin, H.-J.; Lin, J.-D.; Wu, F.-P.; Zhang, Z.; Jiang, Z.-Q.; Zhang, Z.-G.; Gundogdu, K.; et al. A near-infrared non-fullerene electron acceptor for high performance polymer solar cells. *Energy Environ. Sci.* **2017**, *10*, 1610–1620. [CrossRef]
36. Liu, D.; Kan, B.; Ke, X.; Zheng, N.; Xie, Z.; Lu, D.; Liu, Y. Extended Conjugation Length of Nonfullerene Acceptors with Improved Planarity via Noncovalent Interactions for High-Performance Organic Solar Cells. *Adv. Energy Mater.* **2018**, *8*, 1801618. [CrossRef]
37. Liang, J.; Yin, P.; Zheng, T.; Wang, G.; Zeng, X.; Cui, C.; Shen, P. Conjugated side-chain optimization of indacenodithiophene-based nonfullerene acceptors for efficient polymer solar cells. *J. Mater. Chem. C* **2019**, *7*, 10028–10038. [CrossRef]
38. Tu, Q.; Ma, Y.; Zhou, X.; Ma, W.; Zheng, Q. Enhancing the Photovoltaic Performance of Ladder-Type Dithienocyclopentacarbazole-Based Nonfullerene Acceptors through Fluorination and Side-Chain Engineering. *Chem. Mater.* **2019**, *31*, 5953–5963. [CrossRef]
39. Yan, C.; Wu, Y.; Wang, J.; Li, R.; Cheng, P.; Bai, H.; Zhan, Z.; Ma, W.; Zhan, X. Enhancing performance of non-fullerene organic solar cells via side chain engineering of fused-ring electron acceptors. *Dyes Pigments* **2017**, *139*, 627–634. [CrossRef]
40. Hsiao, Y.-T.; Li, C.-H.; Chang, S.-L.; Heo, S.; Tajima, K.; Cheng, Y.-J.; Hsu, C.-S. Haptacyclic Carbazole-Based Ladder-Type Nonfullerene Acceptor with Side-Chain Optimization for Efficient Organic Photovoltaics. *ACS Appl. Mater. Interfaces* **2017**, *9*, 42035–42042. [CrossRef]
41. Liu, T.; Gao, W.; Wang, Y.; Yang, T.; Ma, R.; Zhang, G.; Zhong, C.; Ma, W.; Yan, H.; Yang, C. Unconjugated Side-Chain Engineering Enables Small Molecular Acceptors for Highly Efficient Non-Fullerene Organic Solar Cells: Insights into the Fine-Tuning of Acceptor Properties and Micromorphology. *Adv. Funct. Mater.* **2019**, *29*, 1902155. [CrossRef]
42. Yan, C.; Wang, W.; Lau, T.-K.; Li, K.; Wang, J.; Liu, K.; Lu, X.; Zhan, X. Enhancing the performance of non-fullerene organic solar cells via end group engineering of fused-ring electron acceptors. *J. Mater. Chem. A* **2018**, *6*, 16638–16644. [CrossRef]
43. Zhang, J.; Li, Y.; Hu, H.; Zhang, G.; Ade, H.; Yan, H. Chlorinated Thiophene End Groups for Highly Crystalline Alkylated Non-Fullerene Acceptors toward Efficient Organic Solar Cells. *Chem. Mater.* **2019**, *31*, 6672–6676. [CrossRef]
44. Zhao, W.; Li, S.; Yao, H.; Zhang, S.; Zhang, Y.; Yang, B.; Hou, J. Molecular Optimization Enables over 13% Efficiency in Organic Solar Cells. *J. Am. Chem. Soc.* **2017**, *139*, 7148–7151. [CrossRef] [PubMed]
45. Li, S.; Ye, L.; Zhao, W.; Yan, H.; Yang, B.; Liu, D.; Li, W.; Ade, H.; Hou, J. A Wide Band Gap Polymer with a Deep Highest Occupied Molecular Orbital Level Enables 14.2% Efficiency in Polymer Solar Cells. *J. Am. Chem. Soc.* **2018**, *140*, 7159–7167. [CrossRef] [PubMed]

46. Wang, J.; Zhang, J.; Xiao, Y.; Xiao, T.; Zhu, R.; Yan, C.; Fu, Y.; Lu, G.; Lu, X.; Marder, S.R.; et al. Effect of Isomerization on High-Performance Nonfullerene Electron Acceptors. *J. Am. Chem. Soc.* **2018**, *140*, 9140–9147. [CrossRef]
47. Jia, B.; Wang, J.; Wu, Y.; Zhang, M.; Jiang, Y.; Tang, Z.; Russell, T.P.; Zhan, X. Enhancing the Performance of a Fused-Ring Electron Acceptor by Unidirectional Extension. *J. Am. Chem. Soc.* **2019**, *141*, 19023–19031. [CrossRef]
48. Jiang, K.; Wei, Q.; Lai, J.Y.L.; Peng, Z.; Kim, H.K.; Yuan, J.; Ye, L.; Ade, H.; Zou, Y.; Yan, H. Alkyl Chain Tuning of Small Molecule Acceptors for Efficient Organic Solar Cells. *Joule* **2019**, *3*, 3020–3033. [CrossRef]
49. Kim, G.; Sun, C.; Park, J.S.; Lee, H.G.; Lee, D.; Lee, J.; Kim, H.J.; Cho, S.; Kim, Y.; Kwon, S.; et al. Importance of Terminal Group Pairing of Polymer Donor and Small-Molecule Acceptor in Optimizing Blend Morphology and Voltage Loss of High-Performance Solar Cells. *Adv. Funct. Mater.* **2021**, *31*, 2100870. [CrossRef]
50. Lin, Y.; Wang, J.; Zhang, Z.-G.; Bai, H.; Li, Y.; Zhu, D.; Zhan, X. An Electron Acceptor Challenging Fullerenes for Efficient Polymer Solar Cells. *Adv. Mater.* **2015**, *27*, 1170–1174. [CrossRef]
51. Lin, Y.C.; Lu, Y.J.; Tsao, C.S.; Saeki, A.; Li, J.X.; Chen, C.H.; Wang, H.C.; Chen, H.C.; Meng, D.; Wu, K.H.; et al. Enhancing photovoltaic performance by tuning the domain sizes of a small-molecule acceptor by side-chain-engineered polymer donors. *J. Mater. Chem. A* **2019**, *7*, 3072–3082. [CrossRef]
52. Wang, H.-C.; Chen, C.-H.; Li, R.-H.; Lin, Y.-C.; Tsao, C.-S.; Chang, B.; Tan, S.; Yang, Y.; Wei, K.-H. Engineering the Core Units of Small-Molecule Acceptors to Enhance the Performance of Organic Photovoltaics. *Sol. RRL* **2020**, *4*, 2000253. [CrossRef]
53. Meng, D.; Wang, R.; Lin, J.B.; Yang, J.L.; Nuryyeva, S.; Lin, Y.; Yuan, S.; Wang, Z.; Zhang, E.; Xiao, C.; et al. Chlorinated Spiroconjugated Fused Extended Aromatics for Multifunctional Organic Electronics. *Adv. Mater.* **2021**, *33*, e2006120. [CrossRef] [PubMed]
54. Cai, Y.; Meng, L.; Gao, H.; Guo, Z.; Zheng, N.; Xie, Z.; Zhang, H.; Li, C.; Wan, X.; Chen, Y. Achieving organic solar cells with efficiency over 14% based on a non-fullerene acceptor incorporating a cy-clopentathiophene unit fused backbone. *J. Mater. Chem. A* **2020**, *8*, 5194–5199. [CrossRef]
55. Lu, L.; Luo, Z.; Xu, T.; Yu, L. Cooperative Plasmonic Effect of Ag and Au Nanoparticles on Enhancing Performance of Polymer Solar Cells. *Nano Lett.* **2012**, *13*, 59–64. [CrossRef]
56. Koster, L.J.A.; Kemerink, M.; Wienk, M.M.; Maturová, K.; Janssen, R.A.J. Quantifying Bimolecular Recombination Losses in Organic Bulk Heterojunction Solar Cells. *Adv. Mater.* **2011**, *23*, 1670–1674. [CrossRef]
57. Xing, S.; Wang, H.; Zheng, Y.; Yu, J. Förster resonance energy transfer and energy cascade with a favorable small molecule in ternary polymer solar cells. *Sol. Energy* **2016**, *139*, 221–227. [CrossRef]
58. Yao, E.-P.; Chen, C.-C.; Gao, J.; Liu, Y.; Chen, Q.; Cai, M.; Hsu, W.-C.; Hong, Z.; Li, G.; Yang, Y. The study of solvent additive effects in efficient polymer photovoltaics via impedance spectroscopy. *Sol. Energy Mater. Sol. Cells* **2014**, *130*, 20–26. [CrossRef]
59. Suman, S.; Singh, S.P. Impact of end groups on the performance of non-fullerene acceptors for organic solar cell applications. *J. Mater. Chem. A* **2019**, *7*, 22701–22729. [CrossRef]